Laminin-332 coordinates mechanotransduction and growth cone bifurcation in sensory neurons

Li-Yang Chiang, Kate Poole, Beatriz E Oliviera, Neuza Duarte, Yinth-Andrea Bernal-Sierra, Leena Bruckner-Tuderman, Manuel Koch, Jing Hu, Gary R. Lewin

Laminin–332 coordinates mechanotransduction and growth cone bifurcation in sensory neurons

Li–Yang Chiang[1,2], Kate Poole[1,2], Beatriz E. Oliveira[3], Neuza Duarte[1],Yinth Andrea Bernal Sierra[1], Leena Bruckner–Tuderman[4], Manuel Koch[3], Jing Hu[1,5] and Gary R. Lewin[1]

[1]Department of Neuroscience, Max–Delbrück Center for Molecular Medicine and Charité Universitätsmedizin Berlin, Robert–Rössle–Str. 10, Berlin–Buch D–13125 Germany. [3]Institute for Oral and Musculoskeletal Biology, Center for Biochemistry, Department of Dermatology, and Center for Molecular Medicine Cologne, Medical Faculty, University of Cologne, D–50931 Cologne, Germany. [4] Department of Dermatology and Freiburg Institute for Advanced Studies – School of Life Sciences LifeNet, University of Freiburg, Freiburg, Germany. [5]Center for Integrative Neuroscience (CIN), Paul–Ehrlich–Str. 15–17, 72076 Tübingen, Germany

[2]These authors made an equal contribution.

Laminin–332 is a major component of the dermo–epidermal skin basement membrane and maintains skin integrity. The transduction of mechanical force into electrical signals by sensory endings in the skin requires mechanosensitive channels. Here we show that mouse epidermal keratinocytes produce a matrix that is profoundly inhibitory for sensory mechanotransduction and directly show that the active molecular component is laminin–332. Substrate–bound laminin–332 specifically suppresses one type of mechanosensitive current (rapidly–adapting, RA–type) independent of integrin–receptor activation. This mechanotransduction suppression can be exerted locally and is mediated by preventing the formation of protein tethers necessary for current activation. We also show that laminin–332 can locally control sensory axon branching behavior. Loss of laminin–332 in humans leads to increased sensory terminal branching and may lead to a de–repression of mechanosensitive currents. These novel functions for this matrix molecule may explain some of the extreme pain experienced by epidermolysis bullosa patients deficient in laminin–332.

Basement membrane molecules such as laminin are important structural components of the skin[1–4], but also serve as substrates for sensory neurons of the dorsal root ganglia (DRG) to grow in culture[5]. The main function of sensory neurons innervating the skin is to detect and relay relevant sensory stimuli, in particular mechanical stimuli[6]. It has long been known that sensory neurons with a nociceptive function (detecting potentially harmful stimuli) can have their endings in the epidermis[7–9] whereas mechanoreceptor endings (touch receptors) reside exclusively in the dermal layer[9–10]. Interestingly, the matrix environments of the epidermis and the dermis are very distinctive[11]. We showed that mechanosensitive currents required for touch receptor function depend on the presence of a protein tether which may function to couple mechanosensitive channels to a laminin–containing matrix[12]. The tether protein is not required for the mechanosensitivity of most nociceptive sensory neurons. Here we set out to address the idea that sensory mechanotransduction might be modulated by distinct matrix components made by different types of skin cells in different skin layers. We show that epidermal keratinocytes produce a matrix that is non–permissive for mechanotransduction and identify the factor responsible as laminin–332 (formerly known as laminin–5). Laminin matrices doped with small amounts of laminin–332 have a dramatically altered network structure that is non–permissive for tether attachment. We demonstrate a spatially restricted loss of mechanotransduction in neurite segments connected to laminin–332–containing matrices. Mutations in all three genes coding the trimeric laminin–332 protein complex can cause epidermolysis bullosa, a severe inherited skin blistering disease[1, 3]. Human keratinocytes that produce a laminin–332 free matrix have no inhibitory activity on mechanotransduction. We have also discovered an activity of laminin–332 matrix in inhibiting sensory axon bifurcation. Our results reveal novel mechanisms whereby permissive and non–permissive substrates can spatially coordinate mechanotransduction in distinct domains within a single neuron.

Results

Keratinocyte matrix is suppresses mechanotransduction

Using whole–cell, patch–clamp techniques we directly recorded mechanosensitive currents in cultured sensory neurons[12–20]. We first asked whether co–culture of sensory neurons with different cellular components of the skin can modulate the activity of mechanosensitive currents. When sensory neurons are cultured on a laminin substrate, standardly–derived from Engelbreth–Holm–Swarm cells (EHS matrix, henceforth referred to as laminin), more than 90% of the cells exhibit a mechanosensitive current evoked using a small (~740 nm displacement) stimulus to the neurite[12, 14–15]. At least three types of mechanosensitive current can be measured in sensory neurons, classified according to their inactivation time constant τ_1, rapidly–adapting (RA, τ_1<5 ms), intermediately–adapting (IA, τ_1<50 ms) and slowly–adapting (SA, no adaptation during a 230 ms stimulus), (Fig. 1a)[20]. Practically all mechanoreceptors, classified by their very narrow action potential (AP) [13, 15], possess an RA–mechanosensitive current, as do many nociceptive neurons classified by their broad humped APs[13]. The proportion of sensory neurons with an RA–mechanosensitive current was ~44% of the recorded population (32/72 recorded cells on a laminin substrate, Fig. 1a). The next most common current type was the SA–mechanosensitive current (~34%) which is biophysically and pharmacologically distinct from the RA–mechanosensitive current and is only found in nociceptors[15] (Fig. 1a). A minority of nociceptors (~12%) possess an IA–current. When we cultured sensory neurons on a monolayer of primary mouse keratinocytes we noted normal neurite growth and recordings indicated that both nociceptors and mechanoreceptors were present (Fig.1b; Supplementary Table 1 online). However, we found a striking loss of RA–mechanosensitive currents so that more than 43% of the recorded cells had no measurable mechanosensitive current and the proportion of neurons with RA–current was reduced to just 7% of the total (4/43

cells, Fig. 1a). This effect was observed in putative mechanoreceptors as well as nociceptors, as defined by AP configuration[13] (4/5 mechanoreceptors had no mechanosensitive current in keratinocyte co–cultures, the remaining mechano–insensitive neurons were nociceptors). The proportion of neurons with an SA– or an IA–current was unchanged compared to the laminin control.

We next cultured sensory neurons on mouse keratinocyte–derived matrix and also observed a profound loss of the RA–mechanosensitive current, indicating that it is the keratinocyte matrix alone that is inhibitory (Fig. 1a). Although the SA–mechanosensitive current was observed in neurons on keratinocytes and keratinocyte–derived matrix, the kinetics of this current was profoundly slowed compared to controls. Normally, mechanosensitive currents have very short latencies for activation[15]. However, the latency was dramatically increased from ~600 μs to between 3 and 7 ms for SA– and IA–mechanosensitive currents on keratinocytes and on keratinocyte matrix (Fig. 1c,d; Supplementary Table 1 online). In addition, the activation time–constant for the SA–current slowed dramatically and significantly (Fig. 1d, Supplementary Table 1 online). Despite the loss of RA–mechanosensitive current in almost half of the cells cultured on keratinocytes or keratinocyte matrix, the remaining cells displayed mechanically gated currents with peak amplitudes statistically indistinguishable from those found in control cultures (Supplementary Table 1 online).

Laminin–332 suppresses the RA–mechanosensitive current

We screened for molecules present in keratinocyte–derived matrix that might inhibit mechanosensitive currents. We extracted proteins from tissue culture dishes coated with commercially available laminin (EHS–derived), matrix deposited by a monolayer of 3T3 cells and primary mouse keratinocytes. The proteins were run on SDS gels and Western blotting was carried out with antibodies against known matrix components to identify molecules exclusively present in keratinocyte–derived matrix. We, like others,

identified laminin–332 as one molecule specific to keratinocyte–derived matrix[2, 21–22] (Fig. 2a, see supplementary Fig.1 online for the original blot). Laminin–332 is capable of supporting the growth of chick sensory neurons[23] and so we cultivated sensory neurons on purified, human laminin–332 or on matrix made by rat squamous carcinoma cells (SCC25 cells) a rich source of laminin–332[24]. There was no sign that neurochemically distinct sensory neurons grow preferentially on laminin–332 containing substrates (Supplementary Fig. 2 online). Nevertheless, we found that as on the keratinocyte–derived matrix, RA–mechanosensitive currents were lacking in sensory neurons cultured on laminin–332 and this effect was observed in mechanoreceptors (narrow APs) and nociceptors (humped APs) (Fig. 2b). Thus, a laminin–332 containing substrate recapitulated the effect of keratinocyte–derived matrix in suppressing the RA–mechanosensitive current. However, the laminin–332 substrate did not reproduce the kinetic modulation and slowed activation of SA– and IA–mechanosensitive currents that we had observed on a keratinocyte–derived matrix (Fig. 2c, Supplementary Table 2 online).

These effects might be due to the lack of laminin–111 or other laminin isoforms in purified laminin–332 extracts. We therefore mixed laminin–332 with laminin in different molar ratios. We evaluated the suppressive effect of laminin–332 on RA–mechanosensitive currents by determining the number of cells lacking this current on laminin–332/laminin mixtures. Laminin–332, even when diluted to $1/30^{th}$ of that of laminin, still proved nearly as potent as purified laminin–332 in RA–mechanosensitive current suppression (Fig. 2d). Thus laminin–332 may actively suppress the RA–mechanosensitive current. The suppressive effect required properly folded protein as prior denaturation of laminin–332 rendered it ineffective in this assay (Fig. 2d). We also found that the effect of laminin–332 required contact of the neuron with surface–bound protein, as pre–treatment of neurons with soluble laminin–332 had no inhibitory effect on the mechanosensitive current (Supplementary Fig. 3a online). There was also no

effect of keratinocyte conditioned medium on mechanosensitivity in sensory neurons (Supplementary Table 1 online). Mechanosensitive currents were routinely measured while superfusing the cell with 1μM TTX, which may not completely block all voltage–gated sodium channels. With the membrane impermeable local anesthetic QX–314 in the pipette, which blocks all voltage gated sodium channels, mechanosensitive currents were indistinguishable from those found in control experiments, as was the suppression of the RA–mechanosensitive current by 1: 15 laminin–332/laminin mixture (supplementary Fig. 4).

Mechanotransduction tether not supported by Laminin–332

Only substrate–bound laminin–332 had an effect on mechanosensitive currents. We have shown that a 100 nm protein tether linking sensory membranes with a laminin or laminin–111 substrate is necessary for RA–mechanosensitive currents[12]. This led us to hypothesize that the suppression of RA–mechanosensitive currents on laminin–332 containing matrix may be due to lack of tether binding to this substrate. We tested this directly by visualizing the tether protein using TEM. We cultured sensory neurons on control laminin, purified laminin–111, purified laminin–332, and a laminin–332 mixture of 30:1 and used TEM to determine whether protein tethers were present or not. We found that protein tethers with dimensions >75 nm were essentially absent on laminin–332 containing substrates, compared to neurons on laminin or laminin–111 (Fig. 3a Supplementary Table 3 online). We conclude that a laminin–332 containing substrate does not support the attachment of protein tethers necessary for RA–mechanosensitive currents.

Laminin–332 activates integrin signaling primarily via activation of $\alpha_3\beta_1$ and $\alpha_6\beta_4$ receptors[25–28], we thus asked whether the inhibitory effects of laminin–332 require integrin receptors. We used a monoclonal antibody CM6 that blocks the G–domain of laminin–332[29] and completely prevents attachment and growth of sensory neurons on a

purified laminin–332 substrate (Fig. 3b). Nevertheless, antibody treatment of neurons plated on a laminin/laminin–332mixture (15:1 molar ratio) does not block attachment or growth (Supplementary Fig. 4c online, Fig. 3b) presumably because other integrin receptors are engaged by laminin. Nevertheless, under these conditions we found the same suppression of the RA–mechanosensitive current with the CM–6 antibody as in controls (Fig. 3c). The lack of effect of the CM6 antibody was not due a failure of the antibody to recognize the laminin–332 epitope in laminin/laminin–332 mixes (see Supplementary Fig. 5 online).

Laminin–332 acts locally, not globally

To further examine the mechanism of action of laminin–332 we applied the technique of micro–contact printing of substrate proteins[30–31]. We generated cross–hatched grid patterns with laminin stripes in one direction crossed with stripes of either laminin alone or laminin mixed with laminin–332 at 90^{o} to the laminin stripe (laminin–332 henceforth always refers to a mix of laminin: 20 μg/ml; laminin–332: 1.33 μg/ml; Molar ratio 15:1) (Fig. 4c). Strikingly, sensory neurons plated on such grids produce neurites that follow the laminin tracks producing a quadratic meshwork of neurites (Fig. 4a–c). We filled individual neurons with the fluorescent dye Lucifer yellow via the patch pipette to confirm this growth pattern (Fig 4b). When we examined neurons plated on protein stripes with laminin in both directions, a mechanosensitive current could be evoked from neurites of the same cell regardless of stripe orientation (Fig 4e). In contrast, when neurons were cultured on stripes of laminin–332 in one direction and laminin at 90^{o} (laminin/laminin–332 cross–hatch), then RA–mechanosensitive currents were recorded when stimulating the neurite on laminin but rarely on a laminin–332 containing substrate (Fig. 4d,f; Supplementary Table 2 online). This experiment illustrates the exquisite specificity of laminin–332 as the chances of evoking an SA–mechanosensitive current on the laminin versus the laminin–332 stripe were equal (Fig. 4e,f). The width

of neurites on the laminin–332 stripe was thinner compared to on laminin (see below). However, mechanosensitive currents were no harder to evoke from thinner neurites growing on laminin compared to larger ones (supplementary Fig. 6 online). Proteins were printed in quadrants of 25 × 25 μm, thus the inhibitory actions of laminin–332 were restricted to neuritic segments less than 25 μm. Twenty–five micrometres is very small compared to the size of single afferent receptive fields in the skin that can cover an area of several mms^2 [32]. The highly local nature of the RA–current suppression suggests that laminin–332 may block binding of the tether to laminin or promote instability of the tether protein.

Laminin–332 is proteolytically processed leaving the β3 chain intact, but the N–terminal region of the α3 chain is completely processed and the γ2 chain partially processed (close to the coiled–coil region)[33]. To test whether the suppressive activity of the trimeric laminin–332 molecule might reside in one of these N–terminal fragments, we generated human recombinant soluble N–terminal β3 and γ2 chain proteins (without the coiled–coil region). The recombinant proteins were mixed with laminin and used again to generate one stripe of the cross–hatched pattern. However, we found no evidence that either the N–terminal region of the β3 or γ2 proteins could reproduce the activity of laminin–332 on the RA–mechanosensitive current (Supplementary Fig. 3a,b online). The suppressive activity thus probably resides in the coiled–coil region of laminin–332 or in the G1–G3 domain of the laminin α3 chain.

Laminin–332 suppresses sensory axon bifurcation

We noted a further biological effect of laminin–332 after observing neurite growth on the laminin/laminin–332 cross–hatched patterns. Neurites clearly grew preferentially on the stripes that did not contain laminin–332 so that the total neuritic tree was always highly asymmetrical (Fig. 5a–d). To describe the symmetry of growth we calculated the ratio of neuritic length on one direction versus that at 90^o. This ratio was close to 1 (0.96

± 0.05) for the control situation (laminin/laminin stripes), but was highly asymmetrical in the case of the laminin/laminin–332 experiment at 0.20 ± 0.04 (laminin–332 stripe as numerator) and was statistically significant, $p<0.01$ t–test (Fig 5d). Interestingly, this asymmetric growth was not blocked by the CM6 antibody that blocks laminin–332/integrin receptor interactions (Supplementary Fig. 3 online). We also found no evidence that either the N–terminal region of the β3 or γ2 chains of laminin–332 could produce asymmetric growth (Supplementary Fig. 2a,b online). Interestingly, neurons cultivated on stripes of laminin–332 in both directions showed no evidence of asymmetric growth (ratio 0.92 ± 0.14) (Fig. 5d). The latter experiment suggested that only growth cones confronted with a junction between laminin and laminin/laminin–332 behave in a differential manner. We used time–lapse video microscopy and found that in control cultures the growing neurite almost always bifurcated or trifurcated at the junction between laminin stripes (Fig. 5e,f, Supplementary Video 1 online). This behavior was completely different on laminin/laminin–332 patterns, as here growth cones confronted with a laminin–332 containing stripe almost never bifurcated or trifurcated at the junction (Fig. 5e,f, supplementary video 2 online). Instead, sometime after the main neurite passes the junction a collateral branch was formed onto the laminin–332 containing stripe; such events were rare in control experiments (Fig. 5f). The neurites present on the laminin–332 containing stripes were thinner than those on the laminin stripes (Fig. 5g). However, this effect could be assigned to the "collateral" identity of the branch on laminin–332, as neurites were not thinner than on the control laminin when confronted with laminin–332 containing matrix in both directions (Fig. 5g). There was a small, but significant tendency, for the velocity of neurite growth to be slower on laminin–332 containing stripes than on laminin containing stripes (supplementary Fig. 7 online). It appears that laminin–332 can function as a potent brake on growth cone branching (bifurcation or trifurcation), a hitherto unknown function for this laminin isoform.

Laminin–332 structure may control its biological activity

The minimal molar ratios of laminin to laminin–332 that produced a significant suppression of the RA–mechanosensitive currents were 30:1 and 15:1 (Fig. 2d). We therefore used intermittent–contact mode Atomic force microscopy (AFM) to image the topography of the laminin–332 containing matrix surface and compared this to laminin (Fig. 6). Samples for AFM imaging were prepared by printing stripes of laminin onto glass coverslips. The control substrate, EHS–derived laminin, formed a matrix on the surface punctuated by circular areas with either very thin or no matrix coverage. The percentage coverage was around 79% of the printed surface and the average height of the laminin ~6 nm for control laminin (Fig. 6e). The AFM images of laminin–332 containing matrix demonstrated a profound change in the structure of the surface deposited laminin. First, the laminin–332 containing matrix covered a much smaller surface area (between 20 and 50%) as it was punctuated by many more frequent circular gaps than control laminin. Interestingly, the decreased surface coverage effect was quantitatively much larger in the matrix containing a 15:1 compared to 30:1 laminin/laminin–332 molar ratio (Fig. 6d). Finally, the surface structure of matrix containing laminin–332 was much rougher and irregular than that of the control substrate. This extra roughness was reflected quantitatively in a significantly higher mean height of the matrix in laminin–332 containing substrates an effect that was larger with a higher molar ratio of laminin–332 (Fig. 6e). In summary, these results show that the addition of even small amounts of laminin–332 to laminin leads to a profound reorganization of the matrix structure presented to the sensory neuron. Furthermore, the degree of reorganization of the surface structure closely follows the biological effects of the laminin–332 substrate in suppressing functional RA–mechanosensitive currents.

Human laminin–332 deficiency and mechanotransduction

Herlitz–type junctional epidermolysis bullosa is a severe blistering skin disease predominantly caused by mutations in any one of the three genes encoding the subunits of laminin–332[1, 3]. Purified human laminin–111 is supportive for mechanotransduction[12] and also for the tether protein necessary for the RA–mechanosensitive current (Fig. 3) and so we asked if matrix made by human keratinocytes can suppress RA–mechanosensitive currents. Mouse sensory neurons cultivated on human keratinocyte–derived matrix exhibited fewer RA–mechanosensitive currents than on laminin and this was statistically significant (Chi–squared test $p<0.05$)(Fig. 7a,b). Strikingly, both the latency and speed of activation of SA–mechanosensitive currents recorded from neurons on human–derived keratinocyte matrix were dramatically slowed compared to SA–mechanosensitive currents recorded on a laminin–111 substrate (Fig. 7c,d). We next tested the idea that laminin–332 is the only factor in keratinocyte matrix sufficient to suppress the RA–mechanosensitive current. We obtained and cultured keratinocytes from a patient who had suffered from Herlitz–type junctional epidermolysis bullosa (JEB) (see methods and Supplementary Fig. 7 online). We cultured mouse sensory neurons on the JEB–derived matrix and made recordings from these neurons to examine the prevalence of the RA–mechanosensitive current. There was no significant suppression of the RA–mechanosensitive current on JEB–derived matrix (Fig. 7b), which confirmed that laminin–332 is necessary and sufficient for the suppressive effect of keratinocyte matrix on mechanotransduction. Normal human and mouse keratinocyte–derived matrix not only suppressed the RA–mechanosensitive current, but also led to a substantial increase in the latency and a slowing of activation kinetics of the SA–mechanosensitive current in neurons on this matrix (Fig. 1 and 7). Neurons

cultured on JEB–derived matrix still exhibited SA–mechanosensitive currents with delayed activation and slowed activation time constants similar to controls.

Laminin–332 deficiency and altered skin innervation

Our *in vitro* data suggested that the presence of laminin–332 may suppress axonal branching behavior. We used the PGP 9.5 antibody to label sensory fibers in fixed skin biopsies from 4 JEB patients with the same diagnosis and constellation of mutations (see methods) and 3 disease–free control human biopsies. In normal skin thin PGP 9.5–positive fibers can be observed to cross from the dermis to the epidermis and these fibers are usually unbranched (Fig. 8)[34]. The epidermis of JEB patients was not hyper–innervated as the mean density of fibers measured in controls and JEB samples crossing into the dermo–epidermal boundary was not significantly different (Control = 130.3 ± 10.6 neurites/mm^2, n = 152 ; JEB = 143.2 ± 19.2 neurites/mm^2, n = 45). Normally, very few fibers have branches and thus the mean branch number in controls is much less than 1.0 as most fibers do not branch in the plane of section (branch number=0). In contrast, many more fibers in the JEB skin samples showed 1 or even 2 branches close to the dermo–epidermal border and branching frequency was on average doubled in the epidermis (Control = 0.27 ± 0.1 branch points/ neurite, n = 152; JEB skin = 0.54 ± 0.02 branch points/ neurite, n = 59; $p < 0.001$, Student's t–test) (Fig. 8, for example). We also noted an increase in the incidence of fibers running along the dermo–epidermal border in JEB skin (Incidence: Control = 7.5 ± 3%, n = 32; JEB skin = 33.0 ± 13%, n = 46; $p < 0.001$, student's t–test), such "interface" fibers were observed in blistered and in non–blistering regions (Fig. 8). It is possible that a matrix lacking laminin–332 has a profound effect on neurite branching per se. We tested this idea by culturing mouse sensory neurons on a human JEB keratinocyte–derived matrix and compared their branching behavior to that of neurons grown on a healthy human keratinocyte derived matrix. Sensory neurons attached and produced profuse neurite trees on both matrices

but there was no significant difference in the branching index between these two conditions (Supplementary Fig. 9). We also measured the branching and neurite thickness of mouse sensory neurons plated on purified laminin–332 as well as defined mixtures of laminin/laminin–332 (15:1 and 30:1 molar ratios). We found that it was only the purified laminin–332 that had any significant effect on neurite outgrowth and neurons grow normally on laminin/lamnin–332 mixtures (Supplementary Fig. 10). Thus the previously reported effects of laminin–332 on neurite outgrowth[23] may be due to lack of other laminin isoforms in the substrate and not to an inhibitory effect of laminin–332 per se.

Discussion

Our work reveals new and unexpected functions for the heterotrimeric matrix protein laminin–332 in coordinating mechanotransduction and branching of sensory endings in the skin. We found that even very small amounts of laminin–332 can potently suppress the RA–mechanosensitive current in primary sensory neurons. Laminin–332 in the matrix was shown to change the physical structure of the matrix leading to the disappearance of a tether protein necessary for the RA–mechanosensitive current[12]. This mechanism enables a highly local, rather than global, modulation of sensory mechanotransduction. Thus the specific expression of laminin–332 at the dermo–epidermal junction zone enables a precise control of mechanosensitivity of the sensory endings that enter the epidermal layer to contact keratinocytes. We suggest that the local suppression of axonal branching and mechanotransduction at the dermo–epidermal junction functions *in vivo* to prevent hypersensitivity of sensory axons entering the epidermis. Consistent with this hypothesis, it is known that patients suffering from the blistering disease resulting from loss of laminin–332 also suffer severe pain[35–36]. We suggest that the origin of some of this pain may lie in increased branching of epidermal fibers combined with a de–repression of mechanosensitivity.

Our finding of RA–current suppression by laminin–332 is the first example of an inhibitory effect of any laminin on membrane currents. Laminin–332 has an extremely important role in maintaining the structural integrity of the skin as evidenced by the fact that mutations in all three subunits of laminin–332 cause junctional epidermolysis bullosa, a severe, often lethal, inherited skin blistering disease[1, 3]. Little is known about the effects of laminin isoforms on neuronal function, but β2–containing isoforms such as laminin–421 (previously laminin–9) participate in the organization of neuromuscular junction via β2–mediated interactions with the calcium channel $Ca_V2.2$[37], and the same interaction has been proposed to be a stop signal for sensory axon growth in the skin[38]. The mechanism of laminin–332–mediated suppression of mechanotransduction appears to be unique. We show that a laminin–binding tether protein, identified with TEM, is not present on membranes adjacent to a laminin–332 containing matrix (Fig 3a). This tether protein appears to be essential for the RA–mechanosensitive current as its ablation with proteases renders underlying channels completely insensitive to mechanical stimuli[12]. We propose the following model, laminin–332 alters the three dimensional structure of the matrix (Fig. 6), which masks the tether binding site. This mechanism elegantly explains why the powerful suppression of the RA–mechanosensitive current is localized and independent of integrin receptor activation (Fig 3 and 5). The experiments described here provide independent support for the idea that the tether is indeed a necessary prerequisite for the RA–mechanosensitive current. The virtual absence of the tether protein in the plasma membrane adjacent to a laminin–332 containing matrix adds another biochemical feature to this as yet unidentified protein.

We show two distinct effects of keratinocyte–derived matrix on mechanosensitive currents, RA–mechanosensitive current suppression and a profound slowing of the SA–mechanosensitive current (Fig. 1). The SA–mechanosensitive current is developmentally, biophysically and pharmacologically distinct from the RA–

mechanosensitive current[12–13, 15, 17–18, 39] and the activation of the SA–mechanosensitive current seems to be independent of any protease–sensitive links between sensory neurons and the substrate[12]. We did, however, observe a modulation of the SA–mechanosensitive current following protease treatment which dramatically and transiently slowed the latency for current activation[12], an effect resembling that produced by keratinocyte–derived matrix. However, the slowing of the SA–mechanosensitive current on keratinocyte–derived matrix is independent of laminin–332 (Fig. 2, 7). It is thus possible that specific molecular interactions between unknown factors in the keratinocyte matrix and the sensory neuron can modulate the speed of SA–mechanosensitive current activation.

Here we developed a novel micro–contact printing strategy[30] to study local effects of the laminin–332 containing matrix. We showed that RA–mechanosensitive currents in the same cell are only suppressed in neurites on a laminin–332 stripe, but not on the control laminin stripe. However, there was highly asymmetric branching on laminin/laminin–332 grids and this asymmetry arises because of a radically altered growth cone behavior at the junction between laminin and laminin–332 containing stripes. Interestingly, the molecular structure of laminin–332 containing matrix is highly distinctive from laminin (Fig. 6), which suggests that growth cones detect this difference and change their branching behavior accordingly. The molecular mechanism used to control this decision is not known, but might conceivably be based on detection of different forces generated as the growth cone encounters the different surface structures of the two matrices. Consistent with our *in vitro* data we found that sensory fibers at the dermo–epidermal interface, which are most likely nociceptive endings[7–9] branch more often in the skin of patients lacking laminin–332. In addition, we observed many more fibers coursing along the interface on either side of the dermo–epidermal border. Both phenomena are consistent with the idea that the presence of laminin–332 at the dermo–epidermal border is required for coordinating axonal branching and growth.

However, at least some of the branching defects in JEB skin samples could be a consequence of reactive regeneration of fibers in the skin following skin blistering.

In summary, we demonstrate two important new functions for laminin–332 which most likely take place at the dermo–epidermal junction, suppression of mechanosensitivity and of axonal branching. Our data suggest that the absence of laminin–332 in JEB patients will lead to mechanical hypersensitivity of sensory afferents, which may be exacerbated by increased branching of sensory endings in the epidermis. These novel effects of laminin–332 may in part underlie the extreme pain experienced by sufferers of JEB[35–36].

Acknowledgements

We thank members of the Lewin laboratory for advice and comments on the MS. Heike Thränhardt and Anja Wegner provided excellent technical support. We thank Regina Bönsch for performing the Western blot for laminin–332. We also thank Martin Bastmeyer and Anne von Philipsborn for their help in establishing the microcontact printing method in the lab. We are grateful to Bettina Erdmann for help and advice with the TEM experiments. This work was supported by grants from the Deutsche Forschungsgemeinschaft (to GRL and MK) and by the Network Epidermolysis Bullosa grant from the Federal Ministry of Education and Research, BMBF (to LB–T) and a von Humboldt fellowship to JH.

Author contributions

JH and LYC, and KP performed the electrophysiology experiments and LYC carried out the TEM analysis. BEO and MK provided laminin–111/Nidogen complexes, recombinant β3 and γ2. KP carried out microcontact printing with LYC and performed time–lapse experiments. KP carried out AFM experiments, neurite outgrowth assays and human skin immunocytochemistry were performed by KP with help from ND and YABS. LBT provided and characterized the human keratinoctyes. LYC, JH, KP, and GRL planned experiments and analyzed data. GRL and JH wrote the paper.

Author Information The authors declare no competing financial interests. Correspondence and requests for materials should be sent to GRL (glewin@mdc–berlin.de) or to JH (jing.hu@cin.uni–tuebingen.de).

Figure Legends

Figure 1. Keratinocyte–derived matrix suppresses mechanotransduction currents. (a) Example traces of RA, IA and SA mechanosensitive currents evoked by mechanical stimulation of neurites. Stacked histograms show the proportion of the three types of mechanosensitive current observed in neurons recorded on different substrates. Note a dramatic loss of RA–mechanosensitive current in cells cultured on keratinocytes and keratinocyte–derived matrix (number of recorded neurons is indicated above each histogram, $p<0.01$, chi–squared test). (b) Bright field images of sensory neuron cultured on keratinocytes (upper panel). Immunostaining (NF–200) of a neuron cultured on keratinocytes shows the neurite outgrowth (lower panel). RE denotes recording pipette and MS denotes mechanical stimuli. (c) Example current traces of SA–mechanosensitive currents for each culture condition. Note the very long latency and relatively slow activation (mono–exponential fit shown with red line) for inward currents evoked on keratinocytes. (d) Quantitative comparison of the latency and activation time constant of neurons cultured on laminin, keratinocytes and keratinocyte–derived matrix. The latency of SA–mechanosensitive current in keratinocytes co–culture is significantly longer than on laminin. The time constant for SA–mechanosensitive current activation (τ_1) on a keratinocyte monolayer is also significantly longer than on the laminin substrate ($p<0.01$ Mann Whitney U–test). Error bars are ± s.e.m.

Figure 2. Laminin–332 reproduces the suppression of RA–mechanosensitive currents. (a) Western blot analysis showing that laminin–332 is present in the keratinocyte–derived matrix, but not in the EHS–derived laminin nor in 3T3 fibroblast–derived matrix. (b) Laminin–332 selectively suppresses RA–mechanosensitive currents. In mechanoreceptors (neurons with narrow, non–humped spikes), the RA–mechanosensitive current is significantly suppressed by a laminin–332 substrate compared to the laminin control (left panel, $p<0.01$ Fisher's exact test). In the

nociceptor group (neurons with wide, humped AP spikes), the RA–mechanosensitive current is also significantly suppressed by a laminin–332 substrate (right panel, $p<0.01$ Fisher's exact test). (c) Sample SA–mechanosensitive current trace on a laminin–332 substrate (upper panel). Latency and activation time constant for SA–mechanosensitive current is shown for neurons on a laminin–332 or SCC25–derived matrix. (d) Stacked histograms show a dramatic inhibition of RA–mechanosensitive currents when different dilutions of purified laminin–332 were mixed with a constant concentration of laminin. Prior denaturation (boiling) of laminin–332 rendered it ineffective in suppressing RA–mechanosensitive current expression. (Number on top of each histogram denotes the number of recorded neurons (*$p<0.05$ **$p<0.01$ Chi–squared test). Error bars are ± s.e.m.

Figure 3. Laminin–332 containing matrix does not support tether formation and exerts its effect independent of integrin receptors. (a) Example TEM micrographs from cultured sensory neurons plated on one of three types of matrix, laminin (top), laminin–111, and laminin–332 (bottom). Note we observed long tether proteins at the interface between sensory neuron membranes in cultures plated on laminin and laminin–111, but these were rare in neurons plated on laminin–332. Quantification of the electron dense attachments from neurons cultured on laminin and on laminin–332. The length of each measured attachment is plotted in random 2D space to illustrate the range of attachment lengths observed. Each dot represents the measured length of each linking object. It is clear that long, tether like proteins greater than 75 nm on laminin–332 are largely missing (scale bar 100 nm). (b) Monoclonal antibody CM6 blocks the interaction of the integrin–binding G–domain of laminin–332 and completely prevents attachment and growth of sensory neurons on a purified laminin–332 substrate (scale bar is 25 μm) (top). Mixture of laminin–332 with laminin rescues attachment and neuritic growth (bottom). (b) The presence of CM6 does not rescue the suppression of the RA–mechanosensitive current on a mixed laminin/laminin–332 substrate.

Figure 4. Laminin–332 suppression of the RA–mechanosensitive current is local, not global. (a) Light micrograph shows that neurite outgrowth follows the cross–hatched grid patterns with laminin stripes in one direction (green) crossed with stripes of either laminin alone, or laminin mixed with an inhibitory concentration of laminin–332 (purple) at 90^{o} to the laminin stripe (RE recording pipette; MS mechanical stimulation). (b) Each neuron was filled with the fluorescent dye lucifer yellow to confirm this growth pattern and the neurites of such cells were then subjected to mechanical stimulation. (c) Neurons cultured on stripes consisting of laminin:laminin–332 (15:1) in one direction and laminin at 90^{o} (laminin/laminin–332 cross–hatch) in the other direction. (d) The RA–mechanosensitive current was only recorded when stimulating the neurite on laminin (green trace), but rarely when stimulating the same neuritic tree on a laminin–332 containing substrate (purple trace). (e) Mechanosensitive currents could be evoked from neurites on the same cell on protein stripes consisting of laminin in both directions regardless of stripe orientation. (f) RA–mechanosensitive currents evoked from neurites on the same cell are significantly reduced on laminin–332 stripes compared to laminin ($P<0.05$ Chi–square test).

Figure 5. Differential growth behavior on laminin and laminin–332.

(a) Neurites show no directional preference when grown on laminin/laminin cross–hatched patterns, but will preferentially grow along laminin stripes when laminin is crossed with laminin:laminin–332 (15:1) (b). Surfaces patterned with stripes containing laminin–332 in both directions support symmetrical growth (c). In all cases the colored lines within the panels indicate the direction of each substrate (laminin–green; laminin–332–purple), each colored bar is 25 μm. (d) Quantification of the ratio of neurite outgrowth in each direction. The neurite length in each direction was summed and a ratio between the two directions calculated. Note that for neurons grown on laminin/laminin–332 stripes a clear bias was observed for neurite outgrowth along the

laminin substrate. (e) Schemes of branching behaviors observed at branch nodes (data obtained from time–lapse movies). At the node the growth cone can bifurcate or trifurcate (upper panel). Alternatively, a collateral branch may form after the growth cone has extended past the junction (lower panel). (f) Quantification of branching events during neurite outgrowth. Most branching events on the laminin/laminin were bi/trifurcations (40/50), however on the laminin/laminin–332 nodes nearly all events were collateral formation (27/29). (g) Quantification of neurite width. Individual frames from bright–field, time–lapse experiments were analyzed by taking an intensity line scan and determining the width of each neurite at the half maximal intensity. Neurites were binned depending on matrix composition and for cells grown on laminin/laminin matrices, on the nature of the preceding branching event (i.e. bifurcation vs collateralization). The collaterals formed on laminin were not significantly smaller than bi/trifurcation branches on the laminin/laminin pattern but the collateral branch on the laminin–332 stripe was significantly thinner (right). *$p<0.05$ Student's T–test. However, neurites formed on laminin–332/laminin–332 control matrices were the same width as those on laminin/laminin substrates. Error bars are ± s.e.m.

Figure 6 Laminin–332 dramatically alters the network structure of the matrix. Topographic images of the matrix at low (left) and high (right) resolution are shown for control laminin (**a**) and laminin doped with laminin–332 30:1 (**b**) and at a higher molar ratio 15:1 (**c**). Note the irregularity of the surface structure with increasing concentrations of added laminin–332 and that laminin–doped with laminin–332 at 15:1 often shows very little protein coverage within the printed stripe (bottom half panel c, left). Quantification of the percentage coverage in the three situations (d) shows that the surface coverage decreases significantly with increasing ratios of laminin–332. The mean height of the matrix also tended to increase with increasing laminin–332 (e). Statistics are Student's T–test, * $p<0.05$, ** $p<0.01$ *** $p<0.001$. Error bars are ± s.e.m.

Figure 7 Human laminin–332 deficiency sensitizes mechanotransduction.

(a) Example traces of RA, IA and SA mechanosensitive currents evoked by stimulating sensory neurons cultured on human keratinocyte–derived matrix. (b) Stacked histograms of the proportion of the three types of mechanosensitive current observed in neurons recorded on different substrates. On a human laminin–111 substrate, mechanotransduction is robust as compared to neurons on EHS laminin with only a few non–responding cells (2/18) showing that purified laminin–111 is a positive control. Note suppression of RA–mechanosensitive currents in cells cultured on normal human keratinocyte–derived matrix (control matrix; number of recorded neurons is noted on top of each histogram, *$p<0.05$; **$p<0.01$, Chi–squared test). On laminin–332 deficient JEB patient keratinocyte–derived matrix (JEB matrix), neuronal mechanotransduction is sensitized to a normal level as compared to neurons on laminin or on a laminin–111 substrate (data reproduced for comparison from ref[12]). (c) Example traces show typical measurements of current latency for each culture condition. Note the very long latency and relatively slow activation for inward currents evoked on normal human keratinocyte–derived matrix (control matrix) as well as on JEB patient keratinocyte matrix (JEB matrix). (d) Quantitative comparison of the latency and activation time constant of neurons cultured on laminin, control human matrix and JEB matrix. The latency of SA–mechanosensitive current on control matrix is significantly longer than on laminin. Matrix lack of laminin–332 (JEB matrix) does not rescue the alteration of SA–mechanosensitive current gating latency (upper panel; $p<0.01$ Mann Whitney U–test). The time constant for SA–mechanosensitive current activation (τ_1) on both control matrix and JEB matrix was on average longer than on the laminin substrate, but this did

not reach statistical significance (lower panel; Mann Whitney U–test). Error bars are ± s.e.m.

Figure 8. Altered sensory afferent branching in the skin of laminin–332 deficient patients. Tissue sections of biopsies from normal skin (Control) and JEB patient (JEB) skin were labelled using anti–PGP9.5 antibody and imaged with epifluorescence. The number of nerves crossing the dermo–epidermal boundary (marked with yellow, dashed line in all three images), branch points per nerve within the epidermis and the percent of the dermo–epidermal interface innervated were quantified from the images (see text). A typical image from control skin with a white arrow indicating a non–branched fiber, shown on the left. Images from JEB skin (middle, non–blistered region and right a blistered region) with a yellow arrow indicating branched fiber. Many fibers course along the dermo–epidermal boundary in JEB skin and these were termed "interface fibers" and one example is marked with red arrow.

Methods

Cell culture

Primary mouse keratinocytes were cultured as described[40]. Newborn mice were decapitated and their limbs and tails removed. After washing with 70% ethanol, trunk skin was removed, and floated (epidermis upwards) overnight at 4°C in a petri dish containing 0.25% trypsin. On the next day the epidermis was peeled from the underlying tissue. Keratinocytes were harvested from both surfaces of the epidermis by flushing with medium or gentle scraping, harvested cells were then placed in a defined serum–free keratinocyte medium (Gibco–Invitrogen, Germany). After washing, keratinocytes were plated either on glass cover slips pre–coated with 0.67 μg/cm^2

Collagen IV or cultured together with lethally irradiated 3T3 cells acting as an adhesion layer. Squamous cell carcinoma 25 (SCC25) was obtained from ZITHROMAX.

Primary human epidermal keratinocytes from JEB patients were cultured as described [41] from skin of a newborn with extensive skin fragility and blistering or from wild type keratinocytes that were a gift from R.E. Burgeson (Massachusetts General Hospital, Boston US). Around 15,000 wild type and mutant keratinocytes were cultured on glass cover slips for five days in keratinocyte basal medium (Lonza). The cover slips were coated with bovine collagen solution and fibronectin (each 5µg/ml). The cells were then lysed with deoxycholate (DOC) and the remaining matrix was used for further experiments.

Mouse DRGs were dissected and collected in a 1.0 ml tube of PBS on ice. Ganglia were washed once with PBS before incubation with 1µg/ml collagenase type IV in 1ml PBS at 37°C for 30 min. Ganglia were centrifuged briefly (170 x g), the supernatant was removed and DRGs were incubated with 1ml of 0.05% trypsin in PBS, at 37°C for 30 min. The supernatant was removed and a 1ml D–MEM/F12 containing medium was added. The suspension was passed through 1–2 different siliconized Pasteur pipettes to dissociate them into single cells and centrifuged at 170 x g for 4 min. The cells were resuspended in 1ml culture medium and then Cells seeded on the desired substrate (about 60–120 µl of cell suspension per coverslip). After 4 hours, an additional DRG medium was added to the coverslips. Cells were cultured for 12–24h at 37°C in a Steri–Cult 200 incubator. No nerve growth factor or other neurotrophin was added to the medium. To prepare co–cultures, DRG neurons were plated on top of the keratinocytes or 3T3 fibroblasts. Whole–cell recordings began 12 h after plating.

Substrate preparation

For co–culture experiments, DRGs were seeded on coverslips with a monolayer of keratinocytes or 3T3 fibroblasts. For keratinocyte–derived (mouse and human) or SCC–25–derived matrix, the cultured monolayers of cells were treated with 0.5% DOC in hypotonic solution for 5 minutes, cells were washed away and the neurons plated on remaining matrix. To generate a global coating of extracellular matrix components, coverslips were pre–coated with poly–L–lysine (PLL), then coated with matrix by incubating the coverslips for 1 hr at 37ºC in a droplet of liquid containing EHS laminin, laminin–332 or various ratios of both.

Microcontact printing can be pattern surfaces with proteins[30]. Negative silicon masters were provided by Dr. Siegmund Schroeter (Institute of Photonic Technology, Jena, Germany) from which PDMS stamps were cast, as described[30]. To print laminin protein on coverslips, these stamps were covered with a printing ink containing either 20 μg/ml EHS laminin, 20 μg/ml EHS laminin plus 1.33 μg/ml laminin–332 or 20 μg/ml laminin plus 0.67 μg/ml laminin–332 in PBS. The printing ink also contained 2 μg/ml Alexa 488– or Alexa 555– conjugated, goat anti–rabbit antibodies to provide a fluorescent marker for detecting printed regions. The CM–6 monoclonal antibody (sc–32794L, Santa Cruz Biotechnology, Santa Cruz, U.S.A.) was used to block integrin attachment sites on laminin–332. The CM–6 antibody was mixed (at 1.33 μg/ml) with 20 μg/ml EHS laminin and 1.33 μg/ml laminin–332 and then printed on coverslips. Coverslips for stamping were cleaned as previously described[30] and activated with oxygen plasma for 1 min immediately prior to stamping. Stamps covered in printing ink were left at 37°C for 45 minutes, then rinsed with ultrapure water and dried in nitrogen. Immediately after drying, the protein was printed from the stamp onto freshly activated glass coverslips. The printed substrates were then stored dry at 4°C for not longer than 24 hours before use.

Electrophysiology

Whole–cell, patch–clamp recordings were made as previously described[15]. During recordings, cells were kept in extracellular buffer (containing (mM): NaCl 140, $MgCl_2$ 1, $CaCl_2$ 2, KCl 4, glucose 4 and Hepes 10 (pH 7.4)) and electrodes were pre–filled with intracellular solution (containing (mM): KCl 110, Na^+ 10, $MgCl_2$ 1, EGTA 1 and Hepes 10 (pH 7.3)). For most experiments, 0.1% lucifer yellow was included in the electrode to fill the neuron with fluorescent dye. Cells were perfused with drug containing solutions by delivered via a common outlet adjacent to the patched cells (WAS02)[42]. To block the activity of voltage–gated sodium channels either tetrodotoxin (TTX) was prepared to a final concentration of 1 μM in extracellular solution, or 10 mM QX–314 was introduced intracellularly via the patch pipette. Observations were made with an Axiovert 200 microscope equipped with a TILL imaging system (Till Vision GmbH), including the polychome V, a CCD camera and the imaging software TILLvisION. Membrane current and voltage were amplified and acquired using an EPC–10 amplifier sampled at 40 k Hz, acquired traces were analyzed using Fitmaster software (HEKA). For most experiments the membrane voltage was held at –60mV with the voltage clamp circuit. Mechanical stimuli were applied using a heat–polished glass pipette (tip diameter 2–5μm), driven by the MM3A micromanipulator system (Kleindiek), positioned at an approximate angle of 45º to the surface of the dish. There are two different movements for the Nanomotor®: 'fine mode' and 'coarse mode'. Fine mode movement from any position is limited to about 740nm in each direction of the Z–axis (calibrated by a Piezo actuator calibration device LL10PZT (LASERTEX). Coarse mode steps (1 step = 740 nm) can be executed in any direction until the micromanipulator reaches its physical limits. The probe was positioned near the neurite, moved forward in steps of 740 nm for 500 msec and then withdrawn. If there was no response, the probe was moved forward by 1 step in coarse mode. The same procedure was repeated until a mechanically activated inward current was recorded. The probe was moved at a speed of 1.4 mm/ms for fine mode and 7.5 mm/ms for coarse mode. For

the analysis of the kinetic properties of mechanically activated current, traces were fitted with single exponential functions using PulseFit software.

Electron microscopy

DRG neurons were isolated and cultivated on laminin–coated petriPERM dishes using standard culture conditions (petriPERM35, Vivascience AG, Germany). After 24hrs, cells were washed twice with 0.1M cacodylate buffer (Electron Microscopy Sciences, PA, USA), fixed with 2.5% glutaraldehyde for 4 hrs and stained with OsO_4 (Sigma–aldrich Co. Ltd.) in the presence of Ruthenium Red (Fluka) to enhance the electron density of extracellular proteins[43]. The fixed samples were dehydrated through a series of graded ethanol exchanges, infiltrated in a mixture of Poly/BedR 812 epoxy resin and propylene oxide (Polysciences Inc, Warrington, PA), and then embedded in Poly/BedR 812 epoxy resin. Embedded samples were randomly sectioned (50nm thick) then contrasted with uranyl acetate and lead citrate (Serva, Germany) and examined with a Zeiss 910 electron microscope. Digital micrographs were taken with a 1kx1k high speed slow scan CCD camera (Proscan) at an original magnification of 10000 X and analyzed with iTEM software (Olympus Soft Imaging Solutions, Germany). For quantification, all attachments between neurite and underlying substrate were identified and the length of each attachment was measured.

Recombinant proteins and purified laminin–332

The β3 and γ2 short arm laminin cDNAs were amplified by PCR (Herculase Stratagene) and subcloned into a modified episomal expression vector: human laminin β3 chain (NM_001127641; AA: 18–576) including a 3' tandem strepII–tag and human laminin γ2 chain (BC113378; AA: 22 – 631) including a 5' 8 histidine tag as well as a 3' tandem strepII–tag. The expression vectors were transfected into 293–EBNA cells with FuGENE 6 transfection reagent (Roche Diagnostics), and selected clones with the

highest protein expression were expanded for large scale production. The purification of the secreted proteins was performed as previously described[44]. Purified rat laminin–332 was obtained from Chemicon (Germany) and was >95% pure as determined with SDS–PAGE.

Atomic force microscopy

To analyze the structure of laminin–coated surfaces, AFM imaging was conducted using the JPK Nanowizard II (JPK Instruments AG, Berlin, Germany) mounted on a Zeiss 200 inverted light microscope (Carl Zeiss Microimaging GmbH, Jena, Germany). Samples were imaged in intermittent contact mode in air using ACT cantilevers. Images were recorded in both trace and retrace directions to identify artifacts.

Time–lapse video microscopy

To follow neurite outgrowth and bi–furcation, cells were imaged with a 20x objective in ibidi dishes (ibidi GmbH, Martinsreid, Germany) on an Olympus IX81 fitted with an environmental chamber, using the Cell^R software. Bright–field images were acquired every two minutes for between 5–8 hours. Temperature was held constant at 37°C and 25 mM HEPES was added to the medium to maintain stable pH.

Neurite branching analyses

DRG neurons from 4 week old mice were cultured for 24 hours on coverslips coated with a keratinocyte–derived matrix from normal human and JEB patient keratinocytes. Cells were then fixed for 20 min using 4% PFA, permeabilized with 0.5% TX–100 and labelled using a rabbit polyclonal primary antibody against PGP9.5 (Ultraclone) at a dilution of 1:1000 for 1 hr at room temperature. An Alexa488–conjugated goat anti–rabbit secondary antibody (1:1000) was used to visualize DRG cells. Labelled cells

were imaged with epifluorescence, using a 20x objective and analyzed using the automated analysis functions of the IMARIS software.

To compare neuritic trees, fixed and stained neurons as described above were imaged using a 20x objective and epifluorescence. A Sholl analysis was conducted using the ImageJ Plugin developed by the Ghosh Laboratory (University of California, San Diego). To measure neurite widths a line scan of intensity values in a bright–field image was taken perpendicular to the length of the neurite, and the full width at half maximum was calculated from a Gaussian fit of these intensity values.

Testing for JEB–Herlitz

Immunofluorescence staining of a skin biopsy specimens from 4 JEB patients revealed a lack of reactivity with antibodies to the laminin α3, ß3 and δ2 chains (antibodies BM165, 6F12 and GB3, respectively), whereas positive staining was observed with antibodies to other proteins of the dermo–epidermal junction zone, such as collagens IV, VII or α6ß4 integrin (Supplementary Fig. 8 online). The patients were infants with homozygous or compound heterozygous null mutations in the LAMB3 gene[45] and exhibited complete lack of laminin–332 in the skin. This constellation was indicative of junctional epidermolysis bullosa Herlitz, JEB–Herlitz. Control skin was obtained from children who underwent surgery for unrelated diagnostic reasons. In addition, since most patients with JEB–Herlitz have mutations in the *LAMB3* gene encoding the laminin ß3 chain, this gene was analyzed. The screening disclosed either homozygosity for the mutation R635X, or compound heterozygosity for the mutations R635X and R42X in the probands[45].

Immunohistochemistry on human skin samples

Skin biopsies from control human skin and JEB patient skin were fixed in 4% PFA for 2 hours, mounted into TissueTek medium and processed as 30 μm thick sections on gelatin coated slides. Before antibody labeling, an antigen retrieval step was performed by placing the slides in citrate buffer, pH 6.0, for 30 min, at 90°C. To label nerves in the skin sections a rabbit polyclonal primary antibody against PGP9.5 (Ultraclone) was used (1:200 for 1 hr at room temperature). The secondary antibody was an Alexa647–conjugated goat anti–rabbit antibody (1:500 for 2 hours at room temperature). All slides were masked and visualized blind, using bright field and epifluorescence microscopy. The area of the interface between dermis and epidermis was calculated from the bright–field images and the number of nerves crossing this interface was counted from the epifluorescent images. In addition, the number of branch points within the epidermis was calculated.

Statistics

Statistical analysis was done using the Graph pad prism, all means are mean ± s.e.m.

References

1. Aumailley, M., Has, C., Tunggal, L. & Bruckner–Tuderman, L. Molecular basis of inherited skin–blistering disorders, and therapeutic implications. *Expert reviews in molecular medicine* **8**, 1–21 (2006).
2. Marinkovich, M.P. Tumour microenvironment: laminin 332 in squamous–cell carcinoma. *Nat Rev Cancer* **7**, 370–380 (2007).
3. Uitto, J. & Richard, G. Progress in epidermolysis bullosa: genetic classification and clinical implications. *American journal of medical genetics* **131C**, 61–74 (2004).
4. Aumailley, M.*, et al.* A simplified laminin nomenclature. *Matrix Biol* **24**, 326–332 (2005).
5. Tomaselli, K.J.*, et al.* Expression of beta 1 integrins in sensory neurons of the dorsal root ganglion and their functions in neurite outgrowth on two laminin isoforms. *J Neurosci* **13**, 4880–4888 (1993).
6. Lewin, G.R. & Moshourab, R. Mechanosensation and pain. *J Neurobiol* **61**, 30–44 (2004).
7. Kruger, L., Silverman, J.D., Mantyh, P.W., Sternini, C. & Brecha, N.C. Peripheral patterns of calcitonin–gene–related peptide general somatic sensory innervation: cutaneous and deep terminations. *J Comp Neurol* **280**, 291–302 (1989).

8. Zylka, M.J., Rice, F.L. & Anderson, D.J. Topographically distinct epidermal nociceptive circuits revealed by axonal tracers targeted to Mrgprd. *Neuron* **45**, 17–25 (2005).
9. Halata, Z.e.a. The mechanoreceptors of the mammalian skin ultrastructure and morphological classification. *Springer–Verlag Berlin*, 1–75 (1975).
10. Sinclair, D. *Mechanisms of cutaneous sensation* (Oxford University Press, 1981).
11. Bruckner–Tuderman, L. Biology of the extracellular matrix. in *Dermatology* (ed. J. Bologna & J.L. Jorizzo) 1483–1496
(Mosby, London, 2003).
12. Hu, J., Chiang, L.Y., Koch, M. & Lewin, G.R. Evidence for a protein tether involved in somatic touch. *EMBO J* **29**, 855–867 (2010).
13. Lechner, S.G., Frenzel, H., Wang, R. & Lewin, G.R. Developmental waves of mechanosensitivity acquisition in sensory neuron subtypes during embryonic development. *Embo J* **28**, 1479–1491 (2009).
14. Wetzel, C*., et al.* A stomatin–domain protein essential for touch sensation in the mouse. *Nature* **445**, 206–209 (2007).
15. Hu, J. & Lewin, G.R. Mechanosensitive currents in the neurites of cultured mouse sensory neurones. *The Journal of physiology* **577**, 815–828 (2006).
16. Drew, L.J. & Wood, J.N. FM1–43 is a permeant blocker of mechanosensitive ion channels in sensory neurons and inhibits behavioural responses to mechanical stimuli. *Mol Pain* **3**, 1 (2007).
17. Drew, L.J*., et al.* High–threshold mechanosensitive ion channels blocked by a novel conopeptide mediate pressure–evoked pain. *PLoS ONE* **2**, e515 (2007).
18. Drew, L.J., Wood, J.N. & Cesare, P. Distinct mechanosensitive properties of capsaicin–sensitive and –insensitive sensory neurons. *J Neurosci* **22**, RC228 (2002).
19. McCarter, G.C., Reichling, D.B. & Levine, J.D. Mechanical transduction by rat dorsal root ganglion neurons in vitro. *Neurosci Lett* **273**, 179–182 (1999).
20. Hao, J. & Delmas, P. Multiple desensitization mechanisms of mechanotransducer channels shape firing of mechanosensory neurons. *J Neurosci* **30**, 13384–13395 (2010).
21. Masunaga, T*., et al.* Localization of laminin–5 in the epidermal basement membrane. *J Histochem Cytochem* **44**, 1223–1230 (1996).
22. Jensen, K.B., Jensen, O.N., Ravn, P., Clark, B.F. & Kristensen, P. Identification of keratinocyte–specific markers using phage display and mass spectrometry. *Mol Cell Proteomics* **2**, 61–69 (2003).
23. Culley, B*., et al.* Laminin–5 promotes neurite outgrowth from central and peripheral chick embryonic neurons. *Neurosci Lett* **301**, 83–86 (2001).
24. Rousselle, P.G.L., DR Keene and RE Burgeson Kalinin: an epithelium–specific basement membrane adhesion molecule that is a component of anchoring filaments. *Journal of Cell Biology* **114**, 567–576 (1991).
25. Xia, Y., . and Carter, WG. Anchorage Mediated by Integrin a6134 to Laminin–5 (Epiligrin) Regulates Tyrosine Phosphorylation of a Membrane–associated 80–kD Protein. *J. Cell Biol.* **132**, 727–740 (1996).
26. Aumailley, M., El Khal, A., Knoss, N. and Tunggal, L. . Laminin–5 processing and its integration into the ECM. *Matrix Biol.* **22**, 49–54 (2003).
27. Tsuruta, D., Hopkinson, S.B., Lane, K.D., Werner, M.E., Cryns, V.L. and Jones,J.C. . Crucial role of the specificity–determining loop of the Integrin β4 subunit in

the binding of cells to Laminin–5 and outside–in signal transduction. *J. Biol. Chem.* **278**, 38707–38714 (2003).
28. Kariya, Y. & Miyazaki, K. The basement membrane protein laminin–5 acts as a soluble cell motility factor. *Experimental cell research* **297**, 508–520 (2004).
29. Plopper, G.*, et al.* Changes in expression of monoclonal antibody epitopes on laminin–5r induced by cell contact. *Journal of cell science* **109 (Pt 7)**, 1965–1973 (1996).
30. von Philipsborn, A.C.*, et al.* Microcontact printing of axon guidance molecules for generation of graded patterns. *Nature protocols* **1**, 1322–1328 (2006).
31. von Philipsborn, A.C.*, et al.* Growth cone navigation in substrate–bound ephrin gradients. *Development* **133**, 2487–2495 (2006).
32. Lewin, G.R. & McMahon, S.B. Physiological properties of primary sensory neurons appropriately and inappropriately innervating skin in the adult rat. *J Neurophysiol* **66**, 1205–1217 (1991).
33. Amano, S.*, et al.* Bone morphogenetic protein 1 is an extracellular processing enzyme of the laminin 5 gamma 2 chain. *The Journal of biological chemistry* **275**, 22728–22735 (2000).
34. Simone, D.A., Nolano, M., Johnson, T., Wendelschafer–Crabb, G. & Kennedy, W.R. Intradermal injection of capsaicin in humans produces degeneration and subsequent reinnervation of epidermal nerve fibers: correlation with sensory function. *J Neurosci* **18**, 8947–8959 (1998).
35. Herod, J., Denyer, J., Goldman, A. & Howard, R. Epidermolysis bullosa in children: pathophysiology, anaesthesia and pain management. *Paediatric anaesthesia* **12**, 388–397 (2002).
36. Fine, J.D., Johnson, L.B., Weiner, M. & Suchindran, C. Assessment of mobility, activities and pain in different subtypes of epidermolysis bullosa. *Clin Exp Dermatol* **29**, 122–127 (2004).
37. Nishimune, H., Sanes, J.R. & Carlson, S.S. A synaptic laminin–calcium channel interaction organizes active zones in motor nerve terminals. *Nature* **432**, 580–587 (2004).
38. Sann, S.B., Xu, L., Nishimune, H., Sanes, J.R. & Spitzer, N.C. Neurite outgrowth and in vivo sensory innervation mediated by a Ca(V)2.2–laminin beta 2 stop signal. *J Neurosci* **28**, 2366–2374 (2008).
39. Lechner, S.G. & Lewin, G.R. Peripheral sensitisation of nociceptors via G–protein–dependent potentiation of mechanotransduction currents. *J Physiol* **587**, 3493–3503 (2009).
40. Paladini, R.D. & Coulombe, P.A. Directed expression of keratin 16 to the progenitor basal cells of transgenic mouse skin delays skin maturation. *The Journal of cell biology* **142**, 1035–1051 (1998).
41. Verrando, P.*, et al.* Keratinocytes from junctional epidermolysis bullosa do adhere and migrate on the basement membrane protein nicein through alpha 3 beta 1 integrin. *Lab Invest* **71**, 567–574 (1994).
42. Dittert, I.*, et al.* Improved superfusion technique for rapid cooling or heating of cultured cells under patch–clamp conditions. *J Neurosci Methods* **151**, 178–185 (2006).
43. Hasko, J.A. & Richardson, G.P. The ultrastructural organization and properties of the mouse tectorial membrane matrix. *Hear Res* **35**, 21–38 (1988).
44. Gara, S.K.*, et al.* Three novel collagen VI chains with high homology to the alpha3 chain. *The Journal of biological chemistry* **283**, 10658–10670 (2008).

45. Fine, J.D.*, et al.* The classification of inherited epidermolysis bullosa (EB): Report of the Third International Consensus Meeting on Diagnosis and Classification of EB. *J Am Acad Dermatol* **58**, 931–950 (2008).

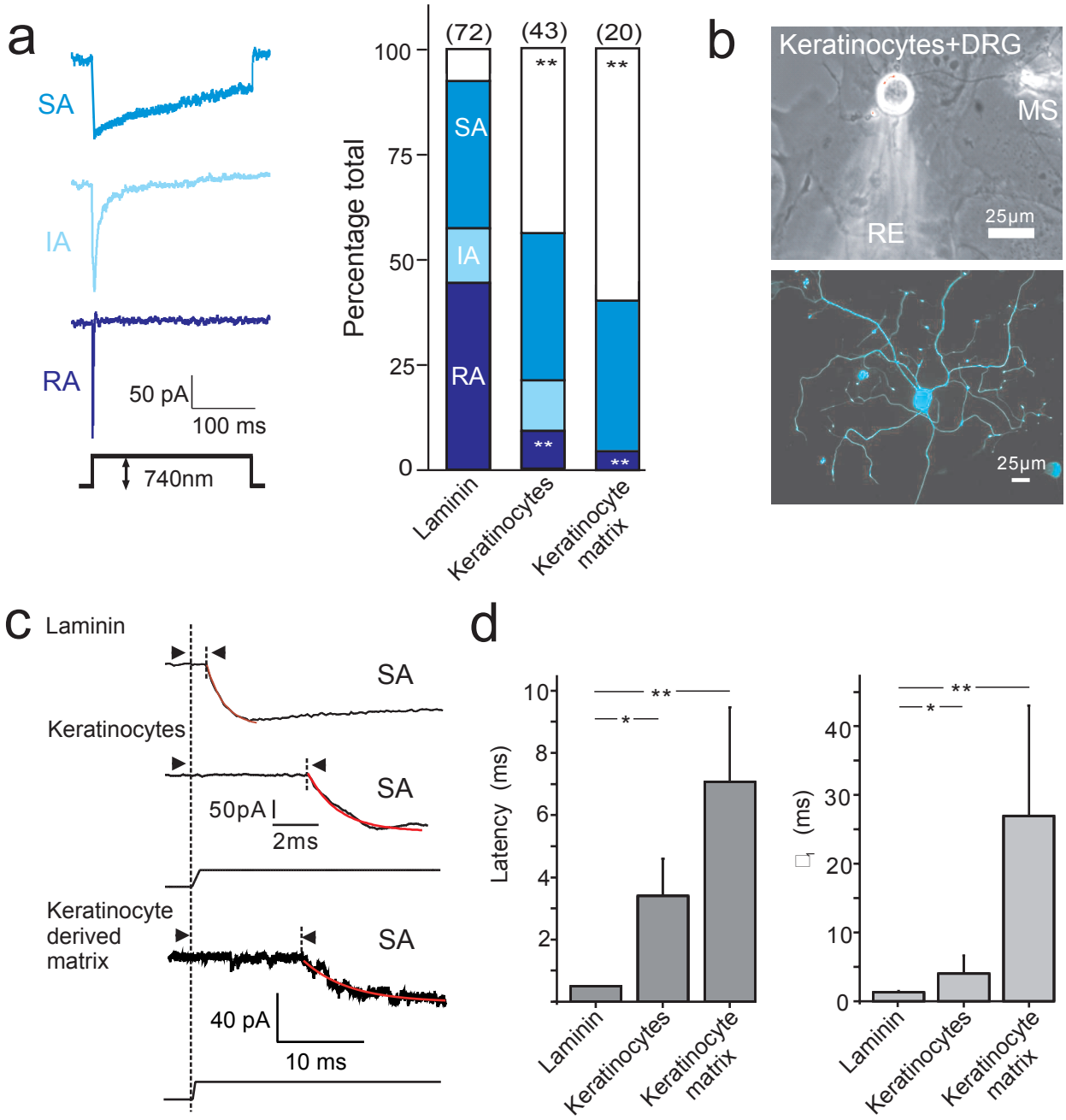

Figure 1 Lewin

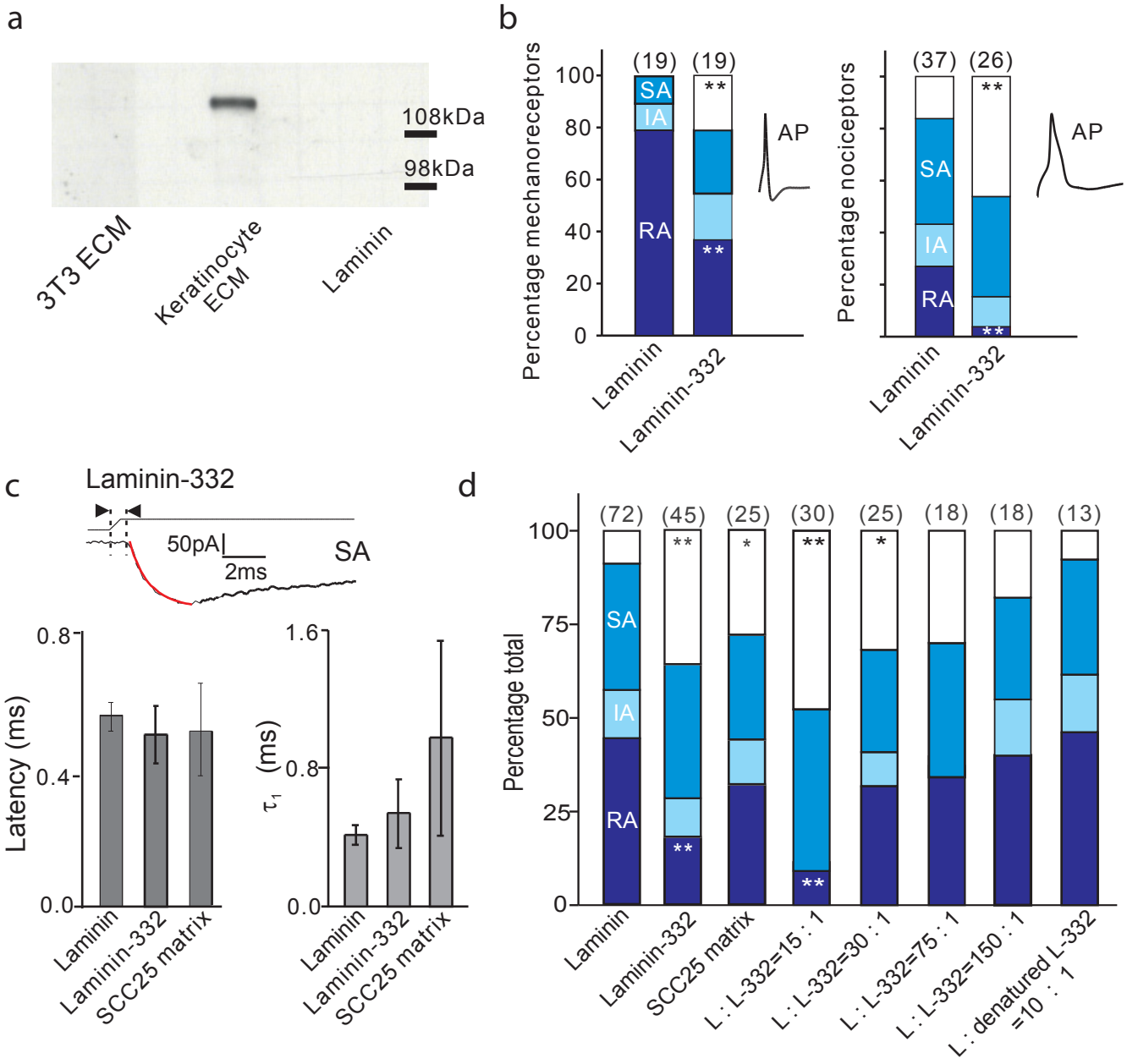

Figure 2 Lewin

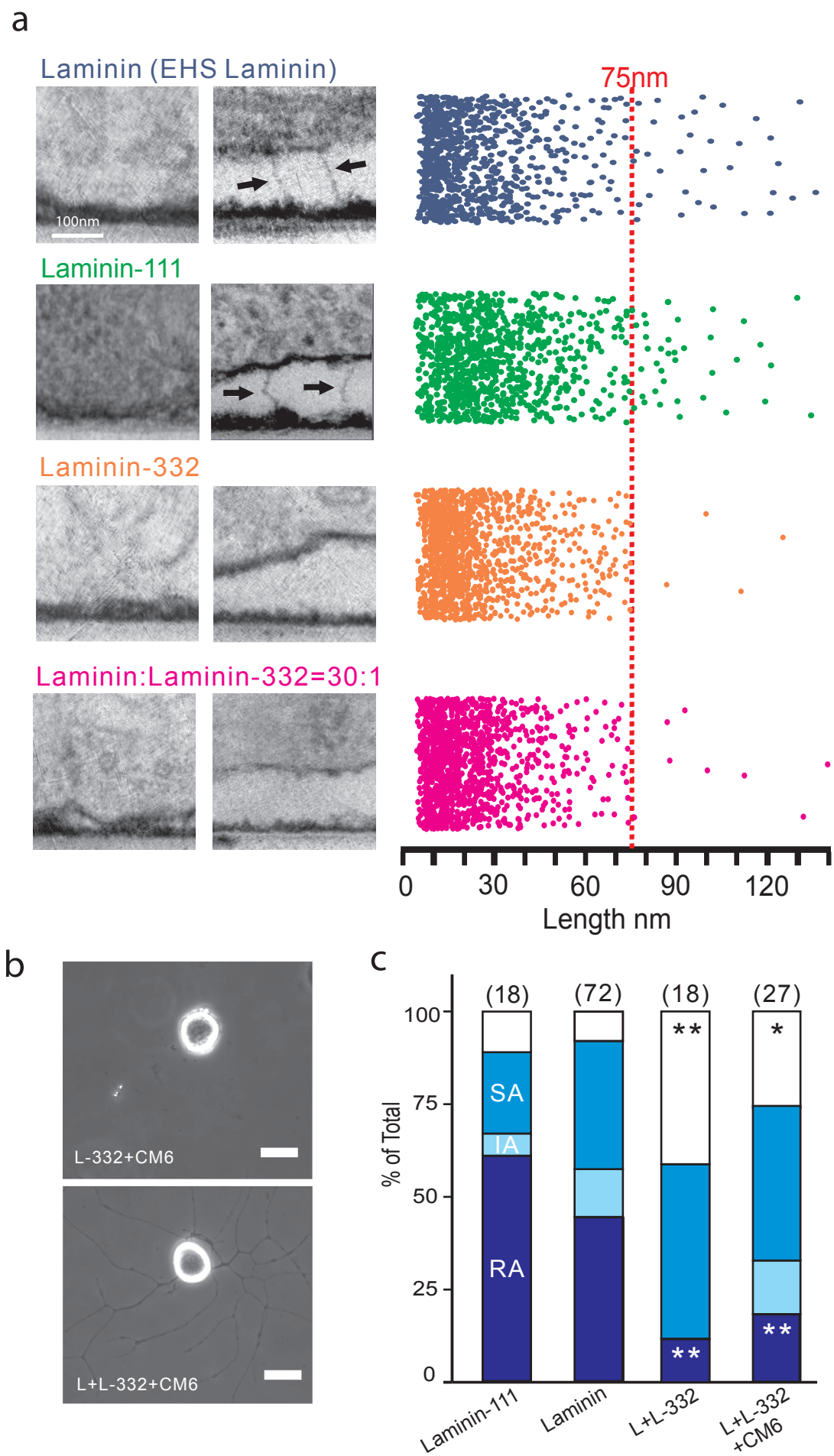

Figure 3 Lewin

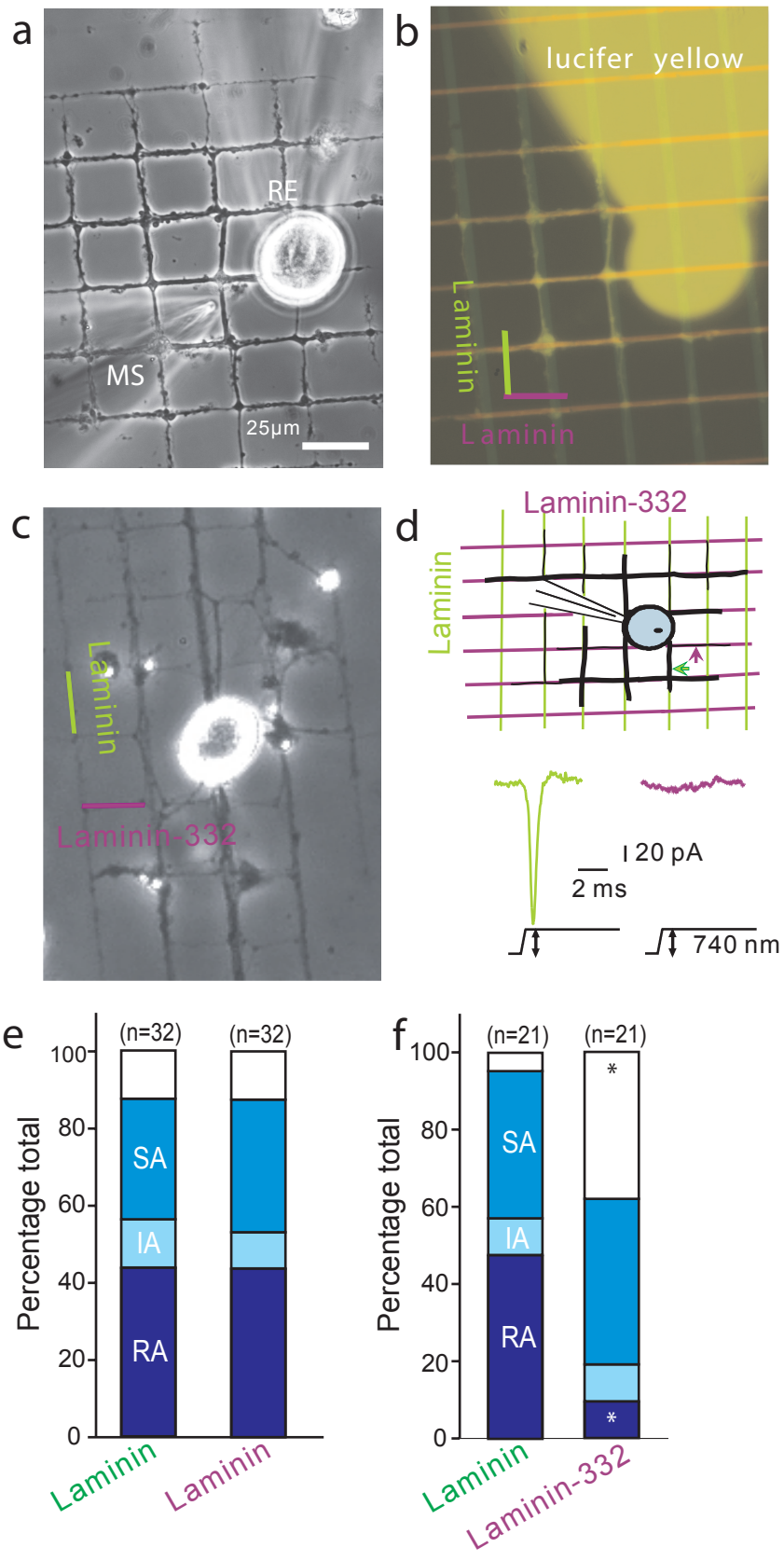

Figure 4 Lewin

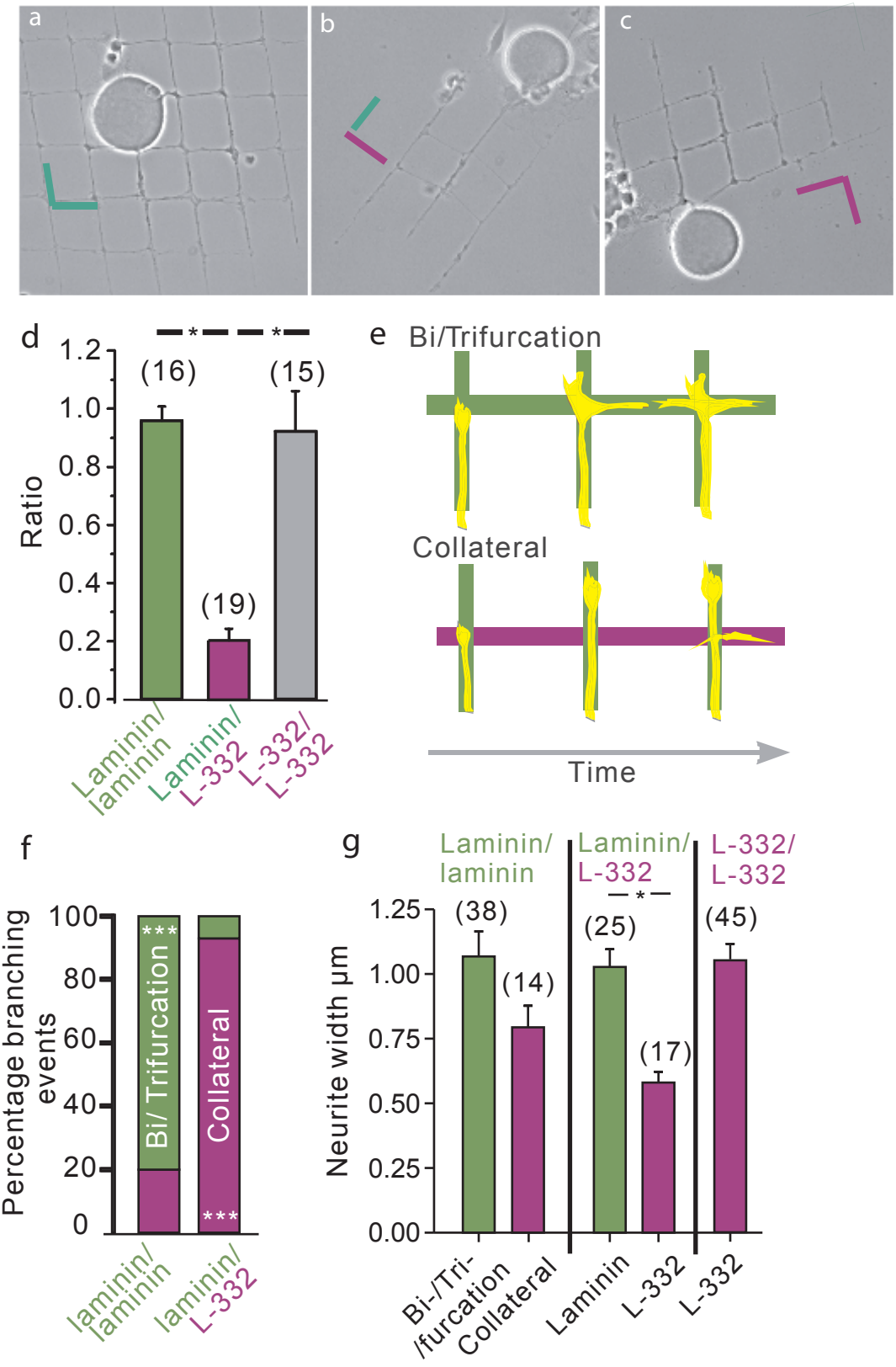

Figure 5 Lewin

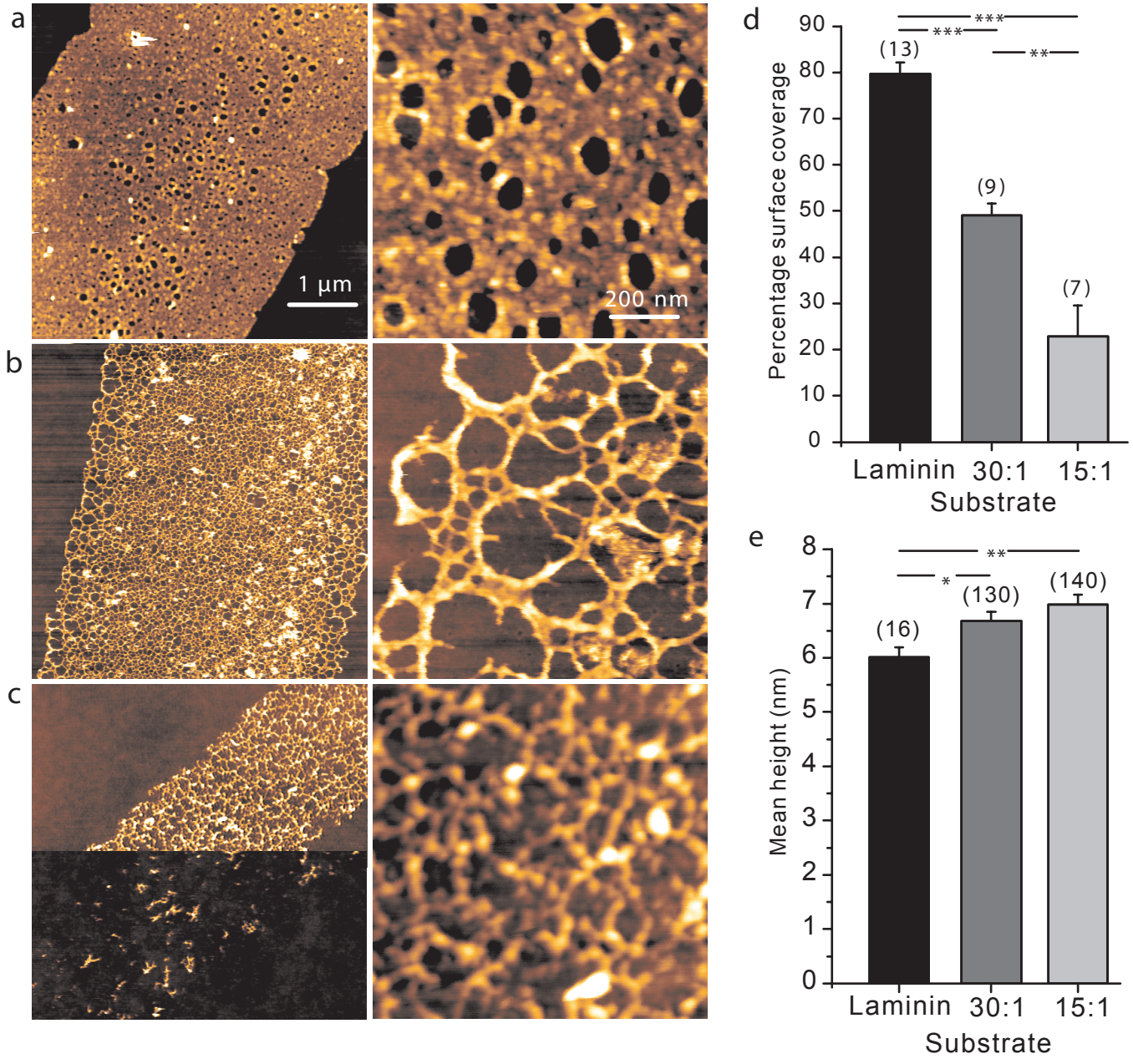

Figure 6 Lewin

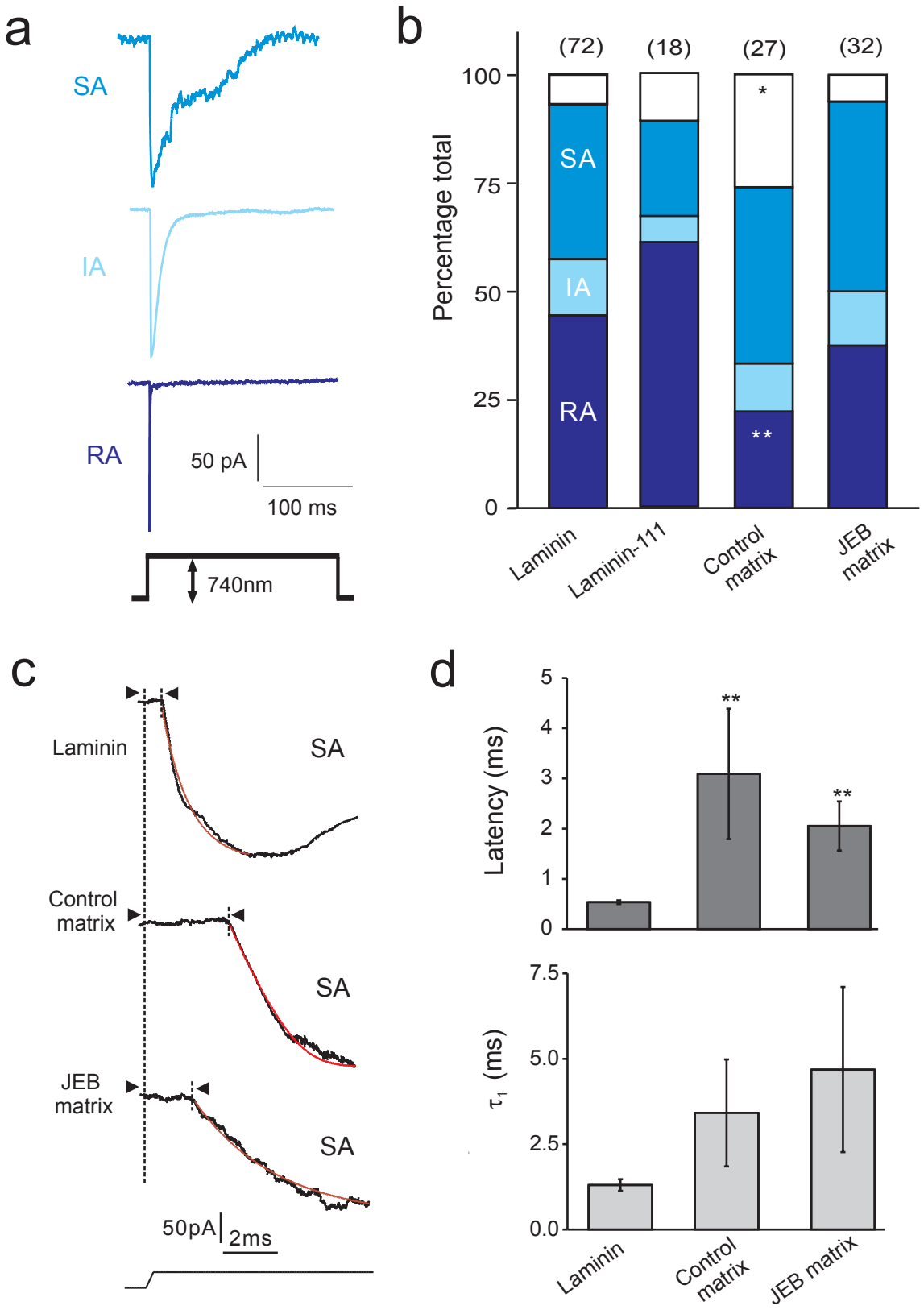

Figure 7 Lewin

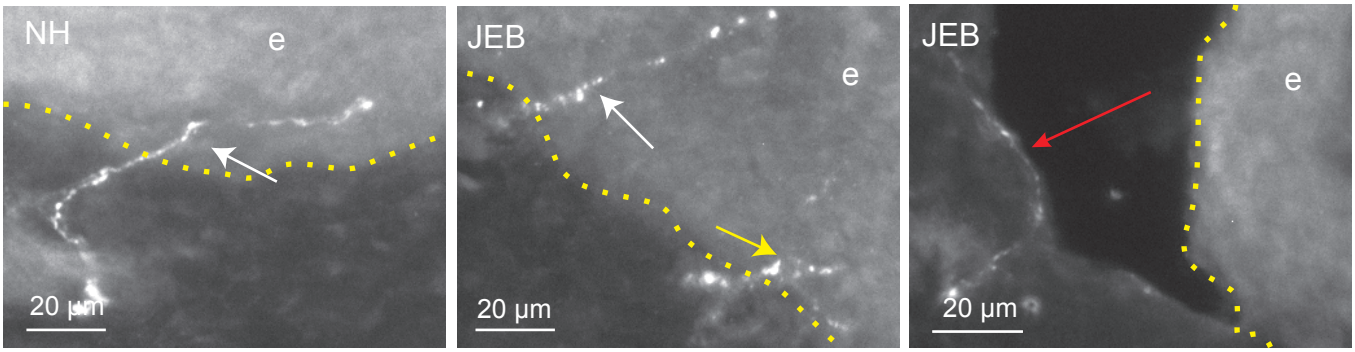

Figure 8 Lewin